Development of Electrical Substitution Fourier Transform Spectrometry for Absolute Optical Power Measurements

J.E. Neira[1]*, S.I. Woods[2], J.E. Proctor[1], J.P. Rice[2]

[1]*Jung Research and Development Corp., Bethesda, MD 20816 USA*
[2]*Sensor Science Division, National Institute of Standards and Technology, Gaithersburg, MD 20899, USA*
** corresponding author: jorge.neira@nist.gov*

Abstract: We have demonstrated the first continuous-scan Electrical Substitution Fourier Transform Spectrometer (ES-FTS), which serves initially as an apparatus for absolute spectral responsivity calibrations of detectors over the wavelength range from 1.5 µm to 11 µm. We present data on the realization of a spectral detector-comparator system with high accuracy, high dynamic range, high spectral resolution and fast measurement in the infrared region, which is tied directly to an absolute power scale through electrical substitution. The ES-FTS apparatus employs a commercial Fourier transform spectrometer and a custom electrical substitution bolometer detector to enable spectrally-resolved absolute optical power measurements. A generalization of electrical substitution techniques enables determination of the voltage waveform which must be applied to the bolometer's electrical heater to cancel the optical signal from a Michelson interferometer, in order to quantify the time-dependent optical power incident on the bolometer. The noise floor of the electrical substitution bolometer is on the order of 10 pW/Hz^{½} and its response is expected to be linear from the noise floor to 1 mW. A direct comparison between a pyroelectric standard detector and the Electrical Substitution Fourier Transform Spectrometer has been performed, and experimental results reported here show the great potential for this technique.

1. Introduction

A critical capability at the National Institute of Standards and Technology (NIST) is spectral responsivity calibration throughout the infrared range [1]. The scale defined by this type of calibration serves as the basis for quantifying measurement results across a range of applications in infrared astrophysics, climate remote sensing, missile defense, infrared imaging, and optical characterization of materials. These calibrations are typically carried out using monochromator-based sources, and due to the low throughput of monochromators are made in a low power range which requires transfer detectors with low noise-equivalent power (NEP). Pyroelectric radiometers have been used for traditional monochromator applications to extend responsivity scales to the long-wave infrared. The voltage response of pyroelectric detectors to optical power cannot be predicted based on physical principles, however, so the absolute scale for their power responsivity must always be calibrated by comparison with a primary standard or through electrical substitution using an integrated heater. In addition, typical pyroelectric detectors have NEP on the order of 10 nW/Hz^{½}, which is often too high to enable uncertainties less than 1 %.

The primary standard detector most often used to define an absolute optical power scale is known as an electrical substitution radiometer. By design these radiometers maintain a near-perfect equivalence between changes in optical and electrical power, so their measurements are directly traceable to electrical standards of voltage and resistance. Known as absolute cryogenic radiometers (ACRs) when operated at low temperatures, these devices provide some of the lowest uncertainties for optical power and temperature scale realization [2,3]. Recent advances

have enabled much faster and easily manufacturable ACRs [4,5] which could provide spectral responsivity calibrations with lower uncertainty than pyroelectric detectors, and without the need for a separate optical power scale calibration.

The use of electrical substitution detectors with a Fourier Transform Spectrometer (FTS) has been tried previously in step-scan mode for spectral calibrations [6]. Electrical substitution detectors have also been operated in closed-loop mode for AC calibrations using a chopper to modulate the light [7-9]. The problem with the step-scan mode approach is that for equal data collection times the typical FTS has significantly lower signal-to-noise than when used in conventional continuous-scan mode [10]. The AC calibrations can acquire spectral selectivity when used along with a filter radiometer or monochromator but have lower spectral resolution and throughput than FTS measurements. The time constants for modern ACRs are fast enough for them to be used with continuous-scan Fourier transform spectrometers, so these primary standard detectors have the capacity to be used for FTS absolute spectral responsivity calibrations. In this work, we have developed electrical substitution methods and electronics which allow ACRs to operate in the spectrally multiplexed environment of an FTS.

A helium-cooled electrically substituted bolometer (ESB) developed previously at NIST [11] was chosen to test the feasibility of the Electrical Substitution Fourier Transform Spectrometer (ES-FTS) system. When used in the traditional chopped mode the 8 mm diameter ESB has very low NEP near 10 pW/Hz^{½}. If operated with chopping in closed-loop mode, the ESB has exhibited excellent linearity over a wide dynamic range up to 1 mW. We have successfully developed the first continuous-scan ES-FTS system using this ESB detector. In conjunction with the overall optical and electronic design, a feedback loop methodology was developed and incorporated to achieve closed-loop mode when the source of optical radiation is the interferometrically-modulated beam from an FTS. When operated in closed-loop mode, there is an equivalence between electrical and optical signals, which enables spectrally-resolved absolute optical power to be determined from an AC measurement of electrical power.

The ES-FTS can be used to expand power-responsivity calibrations as well as irradiance-responsivity calibrations in the infrared. We have compared the newly developed ES-FTS with a NIST-calibrated pyroelectric detector, which operates between 1.5 μm to 20 μm and has an optical power uncertainty of approximately 2.5 % (k=2) [1]. The power responsivity scales of the ESB (operating in closed-loop mode) and the calibrated pyroelectric detector have been compared against each other in the 1.5 μm to 11 μm region of spectrum. A detailed description of the methodology, apparatus, experimental procedure, and results are presented in this paper.

2. Spectral Comparator Overall Design

A schematic of the ES-FTS optical layout is shown in Figure 1. M1 and M2 are off-axis paraboloid mirrors, Ap is a 150 μm diameter aperture, M3 is a flat mirror, and M4 is an off-axis paraboloid selector mirror. The detectors shown are the pyroelectric NIST standard (Pyro), and the electrical substitution bolometer (ESB), which is contained in a liquid helium cryostat. The collimated, modulated infrared beam coming from the FTS is directed into the spatial filter optics (M1, Ap and M2), and then the collimated beam from the spatial filter enters the selection mirror optics (M3 and M4). The rotating mirror M4 focuses the beam and selects to which detector the beam is directed. All these fore-optics are shared by both detectors so that the input beams presented to both detectors are as similar as possible, although there is an additional vacuum window after M4 in the case of the ESB. This optical arrangement is well-suited for spectral power responsivity calibrations since both detectors are illuminated in under-filled mode. The FTS, optics, and pyroelectric detector are all in a dry purge gas environment, and the ESB detector is in a vacuum cryostat with a BaF_2 window.

In a Michelson interferometer, a beam of radiation is divided in two paths and later recombined after a path length difference has been introduced by a moving mirror. A condition is thereby created under which interference between the two beams can occur. The intensity variation of the beam emerging from the interferometer can be measured as function of optical

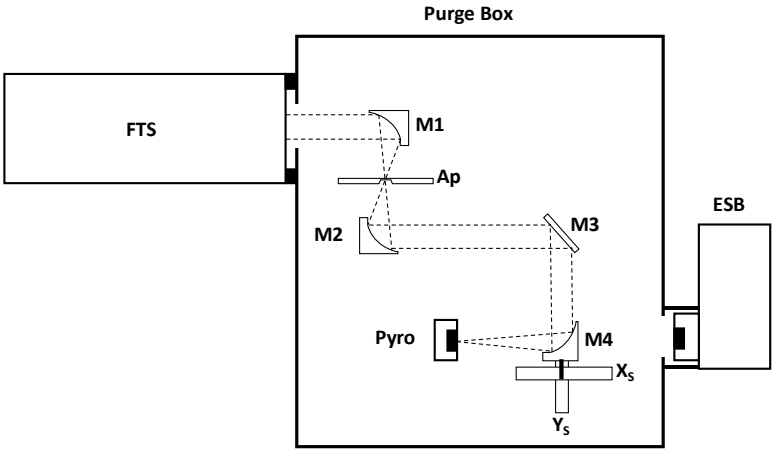

Fig. 1. ES-FTS optical layout. The mirrors (M1-M4), aperture (Ap), and pyroelectric detector (Pyro) are identified in the schematic, in addition to the spectrometer (FTS) and electrical substitution bolometer (ESB). The automated stages (X_S and Y_S) are used to center the beam on either detector.

path difference (OPD) by a detector. For a monochromatic source the signal at the detector can be seen to vary sinusoidally; for a polychromatic source the signal at the detector is seen as an interferogram. In a standard interferometer the beam of a He-Ne (633 nm) laser, known as the "metrology laser", travels through the interferometer, and this laser beam generates sine and cosine timing signals that are captured by two separated silicon photodetectors. A third timing signal, which is a transistor-transistor logic (TTL) signal generated within the FTS, is used to establish the start of an acquisition event as well as the direction of the moving mirror. With these three "metrology signals" a system can extrapolate the start, direction, and the exact position (optical path difference) of the moving mirror at any time.

The complete electronics layout used for our measurements is included in Figure 2. Figure 2a shows the block diagram for the overall ES-FTS electronics wiring, and Figure 2b shows the ESB internal electrical wire diagram. Most of the electronics hardware and the entire software package were developed using off-the-shelf commercial products. The electronics are controlled by a National Instruments (NI) 7931R controller, which is composed of a Field Programable Gate Array (FPGA) and an integrated computer processor, including an attached input-output (I/O) communications module with up to 48 high-speed (100 MHz) digital I/O's. The seven channels of input are based on the Texas Instruments ADS8380 microchip, which is a single-channel high performance 18-bit, 600 kHz analog-to-digital (A/D) converter. The

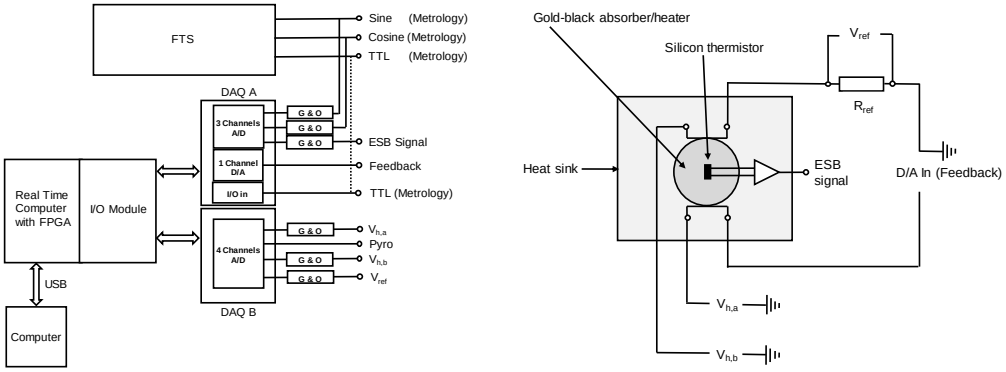

Fig. 2. Schematics of the ES-FTS overall electronics (left) and the ESB detector internal wiring (right). The six boxes labeled "G&O" are gain and offset boards used for preamplification of the signals.

feedback channel is based on the Texas Instruments DAC9881 microchip, which is a single-channel high performance 18-bit, digital-to-analog (D/A) converter. The software user interface and real-time acquisition are programmed using LabVIEW code, and the FPGA and I/O are programmed using the NI FPGA Module with a Xilinx compiler [12]. The FPGA-based data acquisition (DAQ) system is programmed to simultaneously acquire seven A/D input channels as well as supply the single D/A output channel at a sample rate of 100 kHz.

3. ES-FTS Principles of Measurement

3.1 Overview

Under normal operation the ESB can be used to measure the power of a monochromatic well-defined beam, where chopped incident optical power causes heating and cooling of the receiver's gold-black coating layer at the chopper frequency. In closed-loop electrical substitution mode, a feedback current is applied to the ESB receiver heating element to keep its temperature constant, so the optical power is balanced by the applied electrical power. One possible route to make spectral measurements that use an FTS combined with an ESB consists of setting the FTS in step-scan mode and modulating the optical beam from the FTS with a chopper before it reaches the ESB. In this mode the FTS is stopped at each retardation point and the standard closed-loop electrical substitution methodology can be applied to the ESB heating element. Similar to Reference 10, we have found that commercial FTS systems typically exhibit higher noise in step-scan mode than continuous-scan mode. Therefore, in this study we have pursued an electrical substitution technique which is compatible with continuous-scan operation.

The ES-FTS is operated in continuous-scan mode and since the ESB and the pyroelectric detector have slow response times (3dB roll-off frequency < 70 Hz), the FTS mirror velocity is set to 0.03 mm/s. With this slow mirror velocity, the maximum electrical frequency required for the FTS measurement and heater feedback is about 42 Hz for optical wavelengths 1.5 μm and larger. In order to achieve closed-loop mode in the ES-FTS, a new technique was developed to cancel the FTS-modulated interferometric optical signal by applying a synchronized inverse interferometric electrical feedback signal to the bolometer receiver heater element. After achieving optical-electrical power cancellation the system goes into measuring mode, acquiring all the electrical signals necessary to compute the equivalent absolute power spectrum from the ESB. Then the selector mirror turns to the NIST pyroelectric standard detector for comparison.

In measuring mode, the synchronization of the optical IR signal and electrical feedback is accomplished by the FPGA electronics in the following manner. First, a feedback array that represents the inverse interferogram voltage at each value of OPD is uploaded from the computer into the FPGA DRAM memory register. Then, the FPGA data acquisition electronics gathers the ESB signal as well as the sine and cosine metrology signals at 100 kHz to compute the exact mirror position. Next, the FPGA program gathers the appropriate data point from the feedback array stored in memory and it is sent to the D/A feedback channel as output.

3.2 Mathematical Framework

The mathematical approach to determine the correct interferometric feedback signal has been developed using an extension of the Forman method to remove phase error in FTS measurements. In Fourier Transform spectroscopy, the idealized interferogram can be represented by the integral [13]:

$$b_o(\delta) = \int_{-\infty}^{\infty} B(\sigma) e^{-i2\pi\sigma\delta} d\sigma \qquad (1)$$

where $B(\sigma)$ is the optical spectrum of the source as function of wavenumber σ (typically in units of cm^{-1}) and δ is the optical path length difference between the arms of the interferometer (typically in units of cm). The function $B(\sigma)$ is real ($\in \mathbb{R}$), but measured interferograms are typically not symmetric about $\delta = 0$ due to frequency-dependent phase shifts associated with

the interferometer and its acquisition electronics. A more realistic expression for the interferogram, taking into account these phase errors, is:

$$b_\theta(\delta) = \int_{-\infty}^{\infty} B(\sigma) e^{-i\theta(\sigma)} e^{-i2\pi\sigma\delta} d\sigma \tag{2}$$

where $\theta(\sigma)$ is the frequency-dependent phase delay for the FTS measurement. Following the Forman method [14], a simple relation between $B(\sigma)$ and $b_\theta(\delta)$ can be found using standard Fourier-transform identities. Consider the Fourier inverse functions $B(\sigma)$ and $b(\delta)$:

$$B(\sigma) = \int_{-\infty}^{\infty} b(\delta) e^{i2\pi\sigma\delta} d\sigma = \mathcal{F}(b(\delta))$$

$$b(\delta) = \int_{-\infty}^{\infty} B(\sigma) e^{-i2\pi\sigma\delta} d\sigma = \mathcal{F}^{-1}(B(\sigma)) \tag{3}$$

where the notation "$\mathcal{F}$" means "Fourier transform" of the referenced function and "$\mathcal{F}^{-1}$" means the "inverse Fourier transform" of the referenced function. Taking advantage of the convolution (denoted "$*$") and the convolution theorem, one can write:

$$b(\delta) = \mathcal{F}^{-1}\{[B(\sigma)e^{-i\theta(\sigma)}][e^{i\theta(\sigma)}]\} = \mathcal{F}^{-1}[B(\sigma)e^{-i\theta(\sigma)}] * \mathcal{F}^{-1}[e^{i\theta(\sigma)}]$$

$$= (b_\theta * \varphi)(\delta) = \int_{-\infty}^{\infty} b_\theta(\delta')\varphi(\delta - \delta')d\delta' \tag{4}$$

where $\varphi(\delta) = \mathcal{F}^{-1}[e^{i\theta(\sigma)}]$. The measured interferogram is $b_\theta(\delta)$ and the phase function $\theta(\sigma)$ can be found by measuring a low resolution reference interferogram, so the "phase-corrected" interferogram $b(\delta)$ can be readily determined. The phase function is determined by taking the ratio of the imaginary and real parts of $\mathcal{F}[b_\theta(\delta)]$.

In contrast to the phase correction approach, our equations must also include an amplitude gain between the input (optical or electrical signal) and the output (bolometer signal, i.e., change in the bolometer thermistor resistance). Our governing equation for the measured interferogram of the bolometer response is then:

$$b_m(\delta) = \int_{-\infty}^{\infty} B(\sigma)\beta(\sigma) e^{-i\theta(\sigma)} e^{-i2\pi\sigma\delta} d\sigma \tag{5}$$

where $\beta(\sigma)$ is the input-to-output gain, and the phase function $\theta(\sigma)$ includes detector delays in addition to interferometer delays. The gain function $\beta(\sigma)$ is not necessarily linear in input power; in fact, in general it is not linear for a bolometer. The gain function $\beta(\sigma)$ is real ($\in \mathbb{R}$), and we can define the complex gain function $G(\sigma) = \beta(\sigma)e^{-i\theta(\sigma)}$ to express the total effect of the bolometer and interferometer.

3.3. Procedure for Determining Feedback Function

The first step in the determination of the feedback function is to measure bolometer response to a known electrical input to its heater. This measurement is made with no optical signal (i.e., the detector is shuttered or turned away from the optical beam) in order to determine the complex gain function $G(\sigma)$. Using $H(\sigma)$ for the Fourier transform of the voltage applied to the heater, and $h_m(\delta)$ for the voltage measured from the bolometer thermistor, these known quantities obey the following relation:

$$h_m(\delta) = \int_{-\infty}^{\infty} H(\sigma)G(\sigma) e^{-i2\pi\sigma\delta} d\sigma = \mathcal{F}^{-1}(H(\sigma)G(\sigma)) \tag{6}$$

Taking the Fourier transform of both sides of Equation 6 leads to:

$$H_m(\sigma) = \mathscr{F}(h_m(\delta)) = H(\sigma)G(\sigma) \quad \Rightarrow \quad G(\sigma) = \frac{H_m(\sigma)}{H(\sigma)} \tag{7}$$

The second step in determination of the feedback function is to measure the "open loop" optical interferogram signal with no feedback applied and estimate the electrical waveform needed to cancel it. Similar to Equation 4, the relation between the measured interferogram $b_m(\delta)$ and the optical input $b(\delta)$ is:

$$b(\delta) = (b_m * g_{-1})(\delta) = \int_{-\infty}^{\infty} b_m(\delta) g_{-1}(\delta - \delta') d\delta' \tag{8}$$

where $g_{-1}(\delta) = \mathscr{F}^{-1}\left(\frac{1}{G(\sigma)}\right)$

If there is equivalence between electrical and optical heating of the bolometer, then a reasonable first estimate for the electrical heater cancellation interferogram is given by $h_1(\delta) = -b(\delta)$.

The third step in feedback function determination is to apply the electrical feedback $h_1(\delta)$ estimated in step 2 and measure the bolometer interferogram response to the combined optical and electrical signals. Typically, this net signal will not exhibit sufficient cancellation from the first feedback estimate because the bolometer response is not generally linear in applied power and will require further iteration of the process.

The second iteration of the feedback determination starts using the partially cancelled signal (optical + first feedback signal) rather than the optical "open loop" signal. Cancellation in this first estimate is often 95 % or more (of the center-burst amplitude), so the signal to cancel can be < 5 % of the optical signal, and thus the bolometer response in this range is better approximated as linear. The same three steps from the first iteration are repeated: in step 1, a heater waveform with 10 % of the amplitude of that used in the first iteration is applied and a revised complex gain is calculated; in step 2, the electrical feedback function $h_2(\delta)$ is calculated using the revised complex gain; in step 3, the total feedback $h_1(\delta)+h_2(\delta)$ is applied along with the optical signal, and the net bolometer response is measured.

A third iteration of the process can be made, again starting from a smaller initial net signal and calculating a total electrical feedback function $h_1(\delta)+h_2(\delta)+h_3(\delta)$. Usually center-burst cancellation is > 98 % and spectral cancellation is > 99 % by the end of the third iteration. Furthermore, the remaining bolometer resistance signal range can be well-approximated as linear in power, so the process is not extended beyond three iterations.

3.4. Spectral Power Determination

Once the correct electrical heater feedback has been determined for the optical signal, "closed loop" measurements are made with optical and feedback signals applied. The time-dependent current and voltage to the bolometer heater are recorded, as well as the thermistor signal, which in this case has an AC component close to zero. In typical FTS fashion, the signals are averaged as long as necessary to bring the noise level down below a target value.

The expression for the power applied to the ESB electrical heater is:

$$P_{ESB}(\sigma) = \frac{1}{T_w(\sigma) A_{ESB}(\sigma)} \mathscr{F}\left(\left[\frac{V_{ref}(\delta)}{R_{ref}}\right]\left[V_h(\delta)\right]\right) \tag{9}$$

where $V_h(\delta)$ is the interferogram of applied voltage to the heater, $V_{ref}(\delta)$ is the interferogram of voltage across the precision reference resistor in series with the ESB heater, R_{ref} is the resistance

of the precision reference resistor used to determine current through the heater, $A_{ESB}(\sigma)$ is the spectral absorptance of the gold-black absorber of the ESB, and $T_w(\sigma)$ is the spectral transmission of the BaF_2 window on the ESB cryostat. The expression on the righthand side of Equation 9 is phase-corrected using the Forman method in order to remove the effect of measurement-based delays. The bolometer thermistor resistance signal was phase-corrected during the feedback process, but the interferograms associated with the heater signals must also be phase-corrected for the calculation of power.

For our FTS comparison with a calibrated pyroelectric detector, the spectral power measured by this detector is given by:

$$P_{pyro}(\sigma) = \frac{\mathcal{F}\left(V_{pyro}(\delta)\right)}{\mathcal{R}_P(\sigma)\mathcal{R}_\tau(\sigma)} \tag{10}$$

where $V_{pyro}(\delta)$ is the interferogram of the pyroelectric detector voltage signal, $\mathcal{R}_P(\sigma)$ is the calibrated spectral power responsivity of the pyroelectric (in units of V/W), and $\mathcal{R}_\tau(\sigma)$ is its electrical responsivity related to its response time constant [1]. Again, the righthand side of Equation 10 is phase-corrected using the Forman method in order to remove the effect of measurement-based delays. In data collection mode, the detector selection mirror directs the beam to either the ESB or the calibrated pyroelectric detector. Data is measured for about six minutes per detector before returning to the other detector, and this measurement cycle is repeated for up to several hours. For each detector, interferometric data is averaged and postprocessed.

4. Experimental Results

The signal beam from the FTS is centered on the pyroelectric and ESB detectors by adjusting automated stages under mirror M4 in Figure 1. The pyroelectric detector is a square detector 5 mm on a side, and the ESB is a circular detector with an 8 mm diameter. The focused beamspot usually has a diameter less than 1 mm, so all signals were collected in under-filled mode. Continuous-mode FTS data were taken at a He-Ne laser scan rate of 100 Hz, over a spectral range of 900 cm^{-1} to 6600 cm^{-1}, with a spectral resolution of 32 cm^{-1}.

4.1 Determination of the ESB Feedback Function

The ESB feedback function was found by iteration using the 3-step procedure described above. In the data presented below, three iterations were made, and spectral cancellation at the 99.5 % level was achieved.

Iteration one, step one: The rotating mirror M4 was turned to direct the beam upwards so that no FTS optical signal was incident on the ESB detector. An electric impulse was applied to the ESB electrical heater at the center-burst location and the bolometer's thermistor response signal was acquired as shown in Figure 3 (left). These applied and acquired signals were highly over-sampled. The impulse amplitude is 0.03 V with a base line of 0.2 V, and the OPD length of the impulse is 6.33×10^{-5} cm. The optical path difference (OPD) from datapoint to datapoint is 6.33×10^{-8} cm, and the graphs below only show a small portion of the total OPD around the center-burst location. Using these response data, the complex gain function $G(\sigma)$ was calculated using Equation 7.

Iteration one, step two: The rotating mirror M4 was turned to direct the beam to the ESB detector. No AC feedback was applied, but a baseline DC offset voltage of 0.2 V was applied.

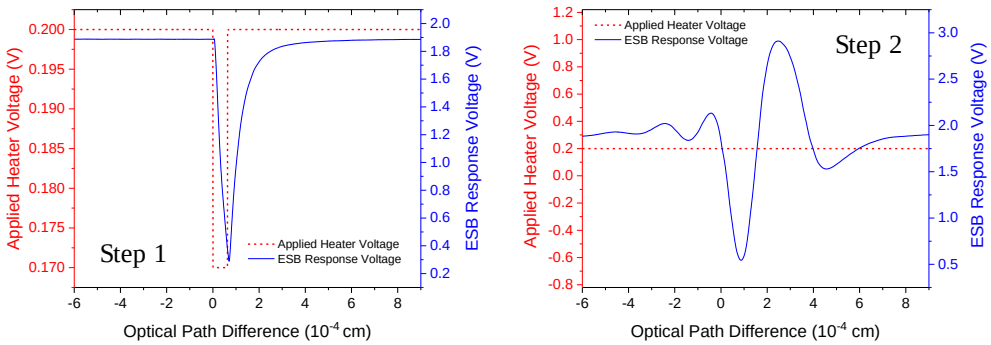

Fig. 3. Iteration 1: step one (left), plots of the electrical impulse applied to the ESB electrical heater (dashed red) and the ESB response (solid blue); step two (right), plots of the DC heater offset (dashed red) and "open loop" interferogram response of the ESB to the optical beam (solid blue).

The "open loop" optical interferogram was acquired, and the first feedback estimate $h_1(\delta)$ was calculated using Equation 8. The applied DC heater signal and "open loop" interferogram response are shown in Figure 3 (right).

Iteration one, step three: With the optical signal still directed to the ESB detector, the first feedback estimate $h_1(\delta)$ was applied to the heater. The level of cancellation in the ESB response was assessed, and another iteration was started if the center-burst amplitude was > 2 % of the "open loop" center-burst amplitude.

Iteration two, step one: The rotating mirror M4 was turned to direct the beam upwards so that no FTS optical signal was incident on the ESB detector. A smaller electric impulse (10 % of that applied in iteration one, step one) was applied to the ESB electrical heater at the center-burst location and the bolometer's response signal was acquired. The applied electrical function and the bolometer's response signal are shown in Figure 4 (left). The impulse amplitude is 0.003 V with a base line of 0.2 V, and the OPD length of the impulse is 6.33×10^{-5} cm. Using these response data, a revised complex gain function $G(\sigma)$ was calculated using Equation 7.

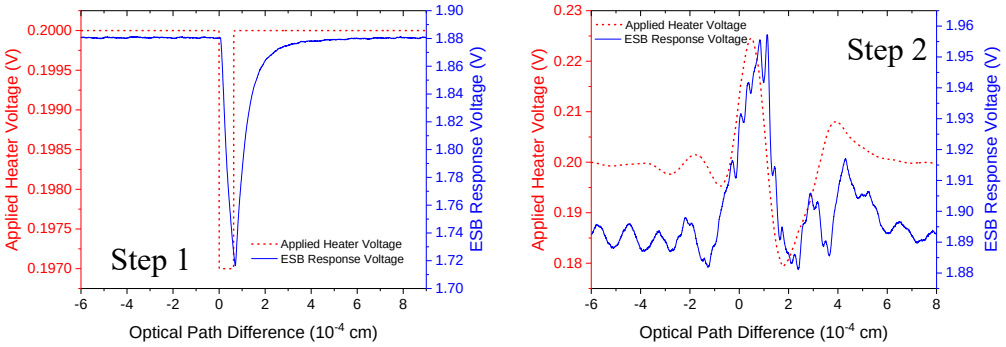

Fig. 4. Iteration 2: step one (left), plots of the electrical impulse applied to the ESB electrical heater (dashed red) and the ESB response (solid blue); step two (right), plots of the applied feedback function (dashed red) and interferogram response of the ESB to the optical beam and feedback (solid blue).

Iteration two, step two: The rotating mirror M4 was turned to direct the beam to the ESB detector. The estimated feedback $h_1(\delta)$ determined in iteration 1 was applied, and the interferogram response of the ESB to the combined input of electrical and optical signal was measured. The measurement configuration was identical to that in iteration one, step three. The applied feedback function and interferogram response of the ESB to the optical beam and feedback are shown in Figure 4 (right). The second feedback estimate $h_2(\delta)$ was calculated using the revised complex gain function and Equation 8.

Iteration two, step three: With the optical signal still directed to the ESB detector, the second total feedback estimate $h_1(\delta)+h_2(\delta)$ was applied to the heater. The level of cancellation in the ESB response was assessed, and another iteration was started if center-burst amplitude was > 2 % of the "open loop" center-burst amplitude.

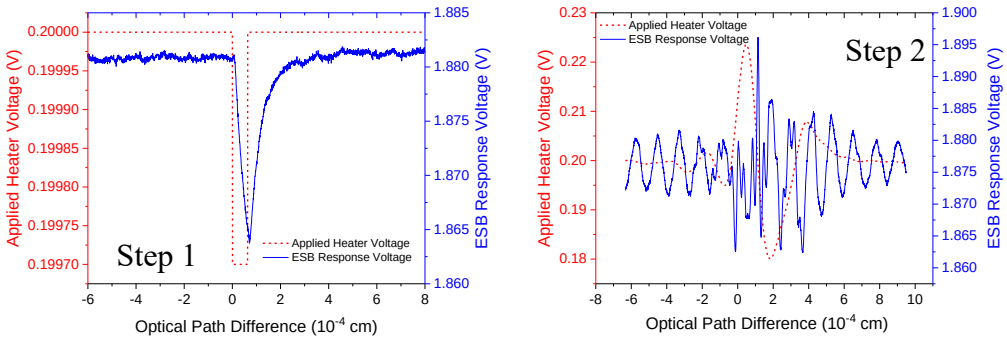

Fig. 5. Iteration 3: step one (left), the electrical impulse applied to the ESB electrical heater (dashed red) and the ESB response (solid blue); step two (right), the applied feedback function (dashed red) and interferogram response of the ESB to the optical beam and feedback (solid blue).

Iteration three: In the third iteration, the same three steps are followed to arrive at the final electrical feedback function $h_1(\delta)+h_2(\delta)+h_3(\delta)$. The results of steps one and two are depicted in Figure 5.

A comparison of the "open loop" (no electrical feedback) response spectrum of the ESB to the optical signal and the "closed loop" response spectrum (using the feedback calculated in iteration 3) is shown in Figure 6. The spectra depicted are from single scans at 32 cm^{-1}

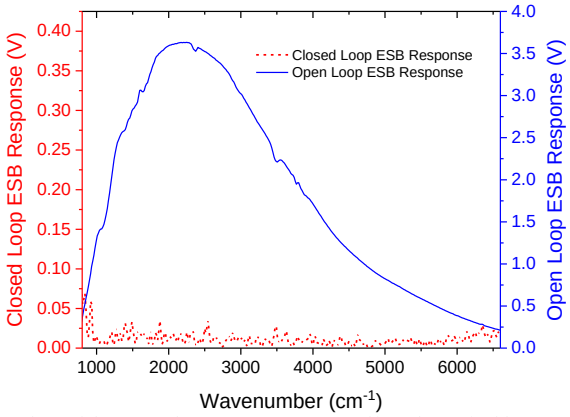

Fig. 6. Plots of the "open loop" ESB spectrum of just the optical beam (solid blue) and "closed loop" ESB spectrum of the optical beam with electrical feedback (dashed red).

resolution (11 seconds per scan). All the interferograms collected in this experiment were phase-corrected using Forman's Method.

4.2. Optical Power Results

After the final feedback function was calculated, the ESB was left in "closed loop" mode and intercomparison measurements began between the ESB and calibrated pyroelectric detector. The time-dependent current and voltage to the bolometer heater are recorded, as well as the thermistor signal, which in this case has an AC component close to zero. The time-dependent AC voltage of the pyroelectric detector was recorded. The base observation time period was 66 seconds, during which time 6 spectra could be co-added, and the dwell time at each detector was 6 base periods. A cycle of measurement, where each detector is exposed to the calibrating beam for 6 base periods, lasts for only 792 seconds, so drift of the spectrometer over time periods longer than 15 minutes does not have a significant effect on the intercomparison. The comparison between detectors was repeated five times for further averaging, so the complete experimental comparison lasted for 3960 seconds.

The spectral absorptance of the gold-black absorber of the ESB, $A_{ESB}(\sigma)$, is approximately 0.99 over the measured spectral range of 1.5 µm to 11 µm. The transmission of the BaF_2 window at room temperature, $T_w(\sigma)$, was measured directly at NIST using an FTS technique. The electrical responsivity $\mathcal{R}_t(\sigma)$ of the pyroelectric detector was approximated by a straight line connecting the measured value at 8000 cm^{-1} (50.6 Hz) to a value of 1.0 at 1000 cm^{-1} (6.33 Hz). The optical responsivity $\mathcal{R}_P(\sigma)$ of the pyroelectric detector was calibrated by the Infrared Spectral Calibration Facility (IRSCF) at NIST. The ESB power was calculated using only the current-voltage data according to Equation 9, without accounting for the small (< 1 %) uncancelled leftover.

The excellent agreement between the ES-FTS power calibration and the calibrated pyroelectric detector measurement of a test infrared signal is shown in Figure 7. Table 1 provides an itemized uncertainty budget for each detector. The Type A statistical error was calculated as the standard deviation of the data over the 5 spectral measurement cycles collected on each detector.

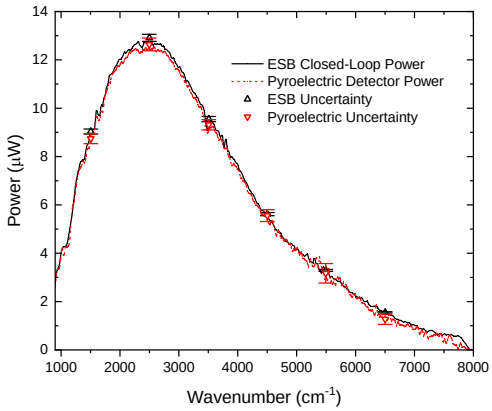

Fig. 7. Plots of the ESB (solid black) and the pyroelectric detector power spectrum (dashed red) on the same scale, with no adjustable parameters. The y-axis shows the power in each wavenumber bin of 32 cm^{-1}. Error bars are shown for both detectors at 6 representative wavenumbers.

5. Discussion

The optical power determined by the pyroelectric detector and the ESB agree within measurement uncertainties over the entire spectrum from 900 cm^{-1} to 6600 cm^{-1}, but the optical

	Pyroelectric	ESB
Type A (at 2500 cm^{-1})	1.42 %	0.13 %
1st Type B	1.1 % ($\mathscr{R}_P$)	1.0 % (A_{ESB})
2nd Type B	1.0 % ($\mathscr{R}_\tau$)	0.5 % (T_w)
Total (at 2500 cm^{-1})	2.1 %	1.1 %

Table 1. Uncertainty budget (coverage k=1) for each detector from near the peak signal at 2500 cm^{-1}.

power determined by the ESB is higher for all wavenumbers, and it is important to carefully investigate sources of error in the measurements. The six representative pairs of error bars in Figure 7 exhibit the agreement of the measurements and also show that the size of the error associated with the pyroelectric detector is significantly larger than for the ESB. In Figure 8, the results are displayed as a ratio of the pyroelectric power to the ESB power, and clearly indicate the agreement of results within uncertainties as well as the systematically lower value of the measured pyroelectric power. The data is shown over the limited range 1700 cm^{-1} to 4300 cm^{-1} because the pyroelectric detector percentage Type A uncertainty increases significantly outside this subrange.

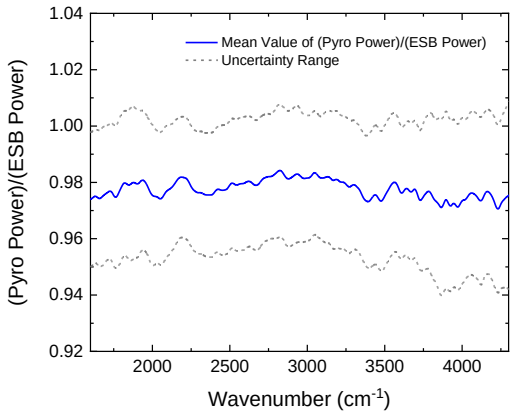

Fig. 8. Plot of the ratio of pyroelectric power to ESB power. The uncertainty range is a combined uncertainty which includes all uncertainties for both the pyroelectric and ESB measurements.

As shown in Table 1, the Type A (statistical) uncertainty near the signal peak for the pyroelectric detector is more than 10 times larger than the Type A uncertainty of the ESB. The difference is even more marked away from the peak: at 5000 cm^{-1} the pyroelectric Type A uncertainty is around 22 times larger and at 1000 cm^{-1} is around 31 times larger. The raw sensitivity of the ESB is at least 100 times better than that of the pyroelectric detector, so as spectral signal drops to levels near the noise floor of the pyroelectric detector, the ESB significantly outperforms the pyroelectric detector in the Type A percentage uncertainty. Due to its relatively low sensitivity, the combined uncertainty for a pyroelectric detector power calibration of this type will always be larger than 1.7 %, given that the calibrated optical responsivity ($\mathscr{R}_P$) has an uncertainty of at least 1 %. On the other hand, for the ESB the minimum combined uncertainty could be approximately 0.2 %, given that more careful

measurements of the gold-black absorptance (A_{ESB}) and BaF_2 window transmission (T_w) could lower the uncertainty on each of those quantities to about 0.1 %.

It is important to consider potential systematic errors in the power calibrations, especially given that the mean power calculated using the ESB is larger than the pyroelectric power for all wavenumbers. In this first version of the ES-FTS data collection system, we could not keep track of the raw data for the "leftover" power after feedback cancellation, so this could lead to a systematic error of up to 1 % (positive or negative) in the recorded ESB power. Another possible source of error is associated with the effects of noise on the deconvolution calculations. It is beyond the scope of this paper, but analysis of how the strength and type of noise affect the ES-FTS method, combined with the use of Wiener deconvolution, will be essential to developing a process which is as robust as possible in the presence of noise. Another possible source of excess signal at the ESB detector could be stray light from the interferometer external to the main optical beam. We have found no evidence for this, but further study of this potential problem is still required.

6. Summary and Conclusions

We have developed a generalized waveform technique for electrical substitution measurements and have successfully applied it to absolute optical power calibrations using a commercial Fourier-transform spectrometer. For calibrations of this type we have improved both sensitivity, by using a cryogenic bolometer rather than a pyroelectric detector, and potential spectral resolution, by employing a Fourier-transform spectrometer rather than a monochromator. In addition, we have lowered the overall uncertainty by using a traceable, self-calibrated primary standard directly for the measurements. This auto-traceability can enable any researcher to make absolute measurements of optical power and fulfills a key modern goal of metrological institutes to develop new detectors and methods to democratize traceability. Further work on the ES-FTS technique will concentrate on the effects of noise on the method, with the goal of developing analysis techniques which are more robust to inherent sources of detector and electronic noise. Cryogenic carbon-nanotube radiometers, which have demonstrated broad sensitivity from the visible to far-infrared, fast time constants, and can be fully manufactured using standard microfabrication techniques, are a natural candidate for the detector to pair with the ES-FTS method in future calibrations.

Acknowledgements. Slava Podobedov and George Eppeldauer from NIST Gaithersburg calibrated the reference pyroelectric detectors used in this study. We would like to acknowledge valuable discussions with John Lehman, Michelle Stephens, Nathan Tomlin, and Malcolm White from NIST Boulder.

Disclosures. The authors declare no conflicts of interest.

Data availability. Data underlying the results presented in this paper are not publicly available at this time but may be obtained from the authors upon reasonable request.

References

1. V.B. Podobedov, G.P. Eppeldauer, and T.C. Larason, "Evaluation of optical radiation detectors in the range from 0.8 μm to 20 μm at the NIST infrared spectral calibration facility," Proc. SPIE 8550, 855029 (2012).

2. J.E. Martin, N.P. Fox, and P.J. Key, "A cryogenic radiometer for absolute radiometric measurements," Metrologia **21**, 147-155 (1985).

3. T.J. Quinn and J.E. Martin, "A radiometric determination of the Stefan-Boltzmann constant and thermodynamic temperatures, between −40 °C and +100 °C," Philos. Trans. R. Soc. Lond. A **316**(1536), 85–189 (1985).

4. N.A. Tomlin, C.S. Yung, Z. Castleman, M. Denoual, G. Drake, N. Farber, D. Harber, K. Heuerman, G.Kopp, H. Passe, E. Richard, J. Rutkowski, J. Sprunck, M. Stephens, C. Straatsma, S. Van Dreser, I.Vayshenker, M.G. White, S.I. Woods, W. Zheng, and J.H. Lehman, "Overview of microfabricated bolometers with vertically aligned carbon nanotube absorbers, AIP Advances **10**, 055010 (2020).

5. J. Lehman, A. Steiger, N. Tomlin, M. White, M. Kehrt, I. Ryger, M. Stephens, C. Monte, I. Mueller, J. Hollandt, and M. Dowell, "Planar hyperblack absolute radiometer", Optics Express, **24**(23), 25911-25921 (2016).

6. H. Latvakoski, G. Cantwell, J.Q. Peterson, and J. Cardon, "RBI ground calibration," presented at the 24th Annual Meeting on Characterization and Radiometric Calibration for Remote Sensing (CALCON), Logan, Utah, 24-27 Aug. 2015.

7. C.A. Hamilton, G.W. Day, and R.J. Phelan, Jr., *An electrically calibrated pyroelectric radiometer system*, NBS Technical Note 678 (National Bureau of Standards, 1976).

8. J. Geist and W.R. Blevin, "Chopper-stabilized null radiometer based upon an electrically calibrated pyroelectric detector," Applied Optics **12**(11), 2532-2535 (1973).

9. Earth Observing System SOlar Radiation and Climate Experiment (EOS SORCE) white paper, "Algorithm theoretical basis document" (Laboratory for Atmospheric and Space Physics, 2000). https://eospso.nasa.gov/sites/default/files/atbd/ATBD-SOR-01.pdf

10. C.J. Manning and P.R. Griffiths, "Noise sources in step-scan FT-IR spectroscopy," Applied Spectroscopy, **51**(8), 1092-1101 (1997).

11. J.P. Rice, "An electrically substituted bolometer as a transfer-standard detector," Metrologia, **37**, 433-436, 2000.

12. Reference is made to commercial products to adequately specify the experimental procedures involved. Such identification does not imply recommendation or endorsement by the National Institute of Standards and Technology, nor does it imply that these products are the best for the purpose specified.

13. P.R. Griffiths and J.A. de Haseth, *Fourier transform infrared spectrometry* (Wiley-Interscience, 2007), Chap. 2.

14. M.L. Forman, W.H. Steel, and G.A. Vanasse, "Correction of asymmetric interferograms obtained in Fourier spectroscopy," J. Opt. Soc. Am. **56**(1), 59-63 (1966).